molecular pharmaceutics

Article

Polymer nanoparticles modified with photo- and pH-dual-responsive polypeptides for enhanced and targeted cancer therapy

Yang Yang, Xiangyang Xie, Yanfang Yang, Zhiping Li, Fanglin Yu, Wei Gong, Ying Li, Hui Zhang, Zhiyuan Wang, and XingGuo Mei

Mol. Pharmaceutics, **Just Accepted Manuscript** • DOI: 10.1021/acs.molpharmaceut.5b00977 • Publication Date (Web): 04 Apr 2016

Polymer nanoparticles modified with photo- and pH-dual-responsive polypeptides for enhanced and targeted cancer therapy

Yang Yang [a], Xiangyang Xie [a,b], Yanfang Yang [a,c], Zhiping Li [a], Fanglin Yu [a], Wei Gong [a], Ying Li [a], Hui Zhang [a], Zhiyuan Wang [a], Xingguo Mei [a,*]

[a] *State key Laboratory of Toxicology and Medical Countermeasure, Department of Pharmaceutics, Beijing Institute of Pharmacology and Toxicology, Beijing 100850, China*

[b] *Wuhan General Hospital of Guangzhou Command，Wuhan 430070, China*

[c] *Beijing Key Laboratory of Drug Delivery Technology and Novel Formulation, Institute of Materia Medica, Chinese Academy of Medical Sciences & Peking Union Medical college, Beijing 100050, China*

Corresponding Author

* Xingguo Mei

Author Contributions

Yang Y. and X.X. contributed equally to this work.

ABSTRACT:

The cationic nature of cell penetrating peptides (CPPs) and their absence of cell selectivity, restrains their applications *in vivo*. In this work, polymer nanoparticles (NPs) modified with photo- and pH-responsive polypeptides (PPPs) were successfully developed, which was respond to near-infrared (NIR) light illumination at the tumor site and a lowered tumor extracellular pH (pHe). In PPPs, the internalization function of CPPs (positively charged) is quenched by a pH-sensitive inhibitory peptide (negatively charged), which is linked via a photo-cleavable group. Small interfering RNA (siRNA) was loaded into NPs by a double-emulsion technique. *In vivo* experiments included siRNA loading, cellular uptake, cell apoptosis, siRNA transfection, tumor targeting delivery, and the *in vivo* antitumor efficacy were carried out. Results showed that the prepared PPP-NPs could selectively accumulated at the tumor sites, and internalized into the tumor cells by the NIR light illumination and the lowered pHe at the tumor site. These studies demonstrated that PPP-NPs are a promising carrier for future tumor gene delivery.

KEYWORDS

Photo- and pH-responsive polypeptides; Cell-penetrating peptides; Small interfering RNA; Tumor targeting nanoparticles

ABBREVIATIONS

CPPs	Cell-penetrating peptides
ACPPs	activable cell-penetrating peptides
PDT	photodynamic therapy

PTA	photothermal ablation therapy
pHe	extracellular pH
PPPs	photo- and pH-responsive polypeptides
EPR	enhanced permeability and retention
siRNA	small interfering RNA

INTRODUCTION

Cell-penetrating peptides (CPPs), which efficiently facilitate the cell uptake of diverse payloads with minor cytotoxicity, have been extensively studied for the delivery of therapeutic agents to cancer cells.[1] However, the cationic nature of CPP that generate both its cell penetrating ability and absence of cell selectivity, hinders its applications *in vivo*. To address this dilemma posed by conventional CPPs, a method using "activable cell-penetrating peptides (ACPPs)" for targeting cargos delivery is encouraging.[2] In ACPPs, the internalization feature generated by poly-cations of CPP was counteracted through covalently attaching a polyanionic inhibitory peptide, which was linking via a divisible enzyme sensitive molecule. Proteolysis of the enzyme sensitive linker that connected the polycationic CPP and the polyanionic inhibitory peptide via certain special enzymes (e.g. matrix metalloprotease-2 and -9) was over-expressed in the tumor site and afforded the separation of both sections and enabled the dissociated CPPs to invade the cells. Although the ACPP-mediated nanocarriers were able to transfer the pharmaceutical molecule into the targeted cells, the application of ACPPs may be limited by the unreliable split of the enzymes and the inadequate departure of the polyanionic inhibitory peptide from the polycationic CPP segment after cleavage.[3, 4] Moreover, the efficient and controlled activity of CPPs via a single-stimuli responsive mechanism in a complex physiological environment without interference still poses a considerable challenge.[5] To overcome this challenge, it is favourable to build a proper delivery system that is based on a dual-stimuli responsive mechanism, which may bring about a feasible protocol for targeted cancer treatment.

Because reliance on the aforementioned enzyme-sensitive cleaving mechanism may

produce some disadvantages, which can be primarily attributed to the vast expression level variations of certain specific enzymes between different individuals,[6, 7] it is desirable to develop a general and triggered cleaving methodology for the nanostructures. Among the general triggers, near-infrared (NIR) light is a favourite triggering stimulus, which possesses good spatial resolution, excellent controllability and non-injury due to its relatively low energy nature. Over the past few decades, NIR light-triggered photodynamic therapy (PDT) and photothermal ablation therapy (PTA) have been developed to treat cancer in a clinical setting.[8] The illumination of NIR light is not only performed at the superficial level of exposure positions such as on the skin, but also at deep-seated tissue by employing a laser head that connected to an endoscope through laparoscopy. Furthermore, more attention is currently focused on the NIR irradiation-induced bond cleavage reaction to establish a platform to control the functions.[9, 10] For example, the release of guest molecules in peptides could be triggered by NIR irradiation using the 4,5-dimethoxy-2-nitrobenzyl group as photo-cleavable molecular gates.[11] Compared with enzyme-sensitive cleaving mechanisms, the cleavable specificities and efficiency of a photo-cleavable group offer modular chemical approaches for the rationally designing of selective cell-penetrating nanostructures, which are specifically and passively activated by the NIR irradiation in the tumor sites. Inspired by these results, we developed a novel polypeptide that is composed of a polycationic CPP that is attached to a polyanionic inhibitory peptide through a photo-cleavable group (4,5-dimethoxy-2-nitrobenzyl group). When then tumor tissue was irradiated with the NIR light, the photo-cleavable group would cleave and thus enabled the activated CPP to invade the cells.

Although these novel polypeptides were efficiently cleaved by NIR irradiation, the polyanionic inhibitory peptide was difficult to separate from the polycationic CPP after cleavage due to an electrostatic attraction.[12] To solve this, we investigated the isoelectric point conversion of an inhibitory peptide that has the potential to eliminate the electrostatic attraction.[13] With the development of a tumor tissue, a lowered tumor extracellular pH (pHe) will emerge. Rapid tumor growth requires a high glycolytic activity, which leads to more lactic acid production and brings a lowered pHe (pH 5.8-7.2) in almost every type of human cancer.[14, 15] Therefore, this point was utilized in our design to establish a pH-sensitive delivery system, and a inhibitory peptide (EEEERRRR) with an isoelectric point of around 6.4 was chosen, which matches the low level pH of the tumor tissue and may reduce the electrostatic attraction at this pH value. The peptide is negatively charged under the physiological conditions (pH 7.4), but it will mostly uncharged or even positively charged at a low pHe.

In this work, a novel delivery tactic was applied in building a new therapeutic agent delivery system by making full use of photo- and pH-responsive polypeptides (PPPs), and this delivery system would transport cargos more selectively and efficiently to tumor cells. The working scheme of the PPP-modified PLGA nanoparticles (PPP-NPs) is shown in Fig. 1. In this system, the PPP includes three elements: a cell-penetrating peptide sequence (CGRRMKWKK), a photo-decomposable group (4, 5-dimethoxy-2-nitrobenzyl group) and a pH-sensitive inhibitory peptide (EEEERRRR). CGRRMKWKK is a CPP that is derived from Penetratin, and it can enhance the membrane translocation efficiency.[16] After systemic administration, PPP-NPs may cumulate at the tumor sites through the enhanced permeability

and retention (EPR) effects. The cell penetration ability of CPPs is effectively shielded by the opposite electric charges within the pH-sensitive inhibitory peptides in circulation. Upon NIR light irradiation at the tumor position, the photo-cleavable group is cleaved. Simultaneously, the pH-sensitive inhibitory peptide eliminates the electrostatic attraction at a lowered pHe. After cleaving the linker and eliminating the electrostatic attraction, the PPP could release its inhibitory peptides to expose the CPPs. Then, with the help of revitalized CPPs, the NPs efficiently enter into the cancer cells. Therefore, the photo- and pH- responsive strategy is planned to amend the targeted delivery efficiency for tumor cells and overcome the shortcomings of single-stimuli responsive mechanism. As the specificity of siRNA-induced gene silencing, the siRNA can be employed as a model drug to evaluate the intracellular delivery efficiency of PPP-NPs. Epidermal growth factor receptor (EGFR), is a cell-surface receptor that is over-expressed in a number of solid tumors, such as anal cancer, lung cancer and glioblastoma multiforme.[17] Based on this, siRNA-loaded nanocarriers for EGFR target was studied in this paper, and their downregulation effects on the target gene was assessed. Here, the physicochemical features of the prepared PPP-NPs for anti-EGFR siRNA was described, then their biological characterizations of were investigated at the cellular level, and their *in vivo* anti-cancer effects was also explored.

■ EXPERIMENTAL SECTION

Materials. 1,2-distearoyl-sn-glycero-3-phosphoethanolamine-N-maleimide (polyethylene glycol) (DSPE-PEG_{2000}-Mal) and 1,2-distearoyl-sn-glycero-3-phosphoethanolamine-N-methoxy (polyethyleneglycol) (ammonium salt) (DSPE-PEG_{2000}) were obtained from Avanti Polar Lipids, Inc. (Alabaster,

AL, USA). PLGA with lactic/glycolic acid ratio (50/50) and 0.55-0.75 dL/g inherent viscosity was obtained from Shandong Institute of Medical Instruments (Shandong, China). Scramble siRNA (sense strand: 5′-UUC UCC GAA CGU GUC ACG UTT-3′; antisense strand: 5′-ACG UGA CAC GUU CGG AGA ATT-3′. entitled as NC-siRNA), anti-EGFR siRNA (sense strand: 5′-AGG AAU UAA GAG AAG CAA CAU dTdT-3′; antisense strand: 5′-AUG UUG CUU CUC UUA AUU CCU dTdT-3′. entitled as EGFR-siRNA) and fluorescein-labeled siRNA (5′ end of the sense strand, FAM-siRNA or Cy5-siRNA) were obtained from GenePharma (Shanghai, China). Fetal bovine serum (FBS) and Dulbecco's Modified Eagle's Medium (DMEM) were purchased from GIBCO, Invitrogen Corp. (Carlsbad, USA). All chemicals were of reagent grade and all purchased from Sigma-Aldrich.

Human breast adenocarcinoma cells (MCF-7 cells) obtained from the Cell Resource Centre of IBMS (Beijing, China) was kept in Dulbecco's modified eagle's medium (DMEM) supplemented with 10% FBS, 100 mg/mL streptomycin, and 100 IU/mL penicillin. The cells were incubated in a humidified incubator (37 °C) with a 5% CO_2 atmosphere.

Female BALB/c nude mice (weighing 18-22 g) were provided by Vital River Laboratories (Beijing, China). The mice were treated in accordance with the requirements of ethics in research, training and testing of animals as laid down by the Animal Care and Use Ethics Committee of Beijing Institute of Pharmacology and Toxicology. The MCF-7 tumor bearing nude mice model was developed as introduced in our previous paper.[18] In short, MCF-7 cells (2×10^6) were injected subcutaneously in the right flank of the mice.

Synthesis of the PPP. Photo-sensitive amino acids (Psaa) were prepared as the previous report of Shigenaga.[11] Briefly, compound **1** and compound **2** were dissolved in DMF and

added to K_2CO_3. Then, the resulting suspension was stirred overnight. An aqueous NH_4Cl solution was added in and kept stirring for 30 min, and deionized water was added in the reaction bottle and extracted with diethyl ether. The diethyl ether phase was rinsed with H_2O, saturated aqueous NH_4Cl solution and brine, dried in vacuum and purified via column chromatography (SiO_2, hexane/AcOEt=20/1) to obtain compound **3**. Compound **3** was dissolved in THF and added to glacial acetic acid and water, and it was stirred for 12 h. The reactant mixture was extracted with AcOEt, dried and purified according to the above steps. The resulting product and PCC were added to dichloromethane and stirred for 6 h. The mixture was filtered through Cerite 535, and the organic layer was handled with a saturated NH_4Cl aqueous solution, dried and purified to obtain compound **4**. $NaClO_2$, 2-methyl-2-butene and sodium dihydrogen phosphate were added to the mixture of acetone/*tert*-BuOH/H_2O (17/12/3 *v*/*v*/*v*, 12.8 mL) with compound **4**. It was stirred for 5 h, a saturated aqueous NH_4Cl solution was added, and it was extracted with AcOEt, dried over Na_2SO_4 and concentrated in vacuum. The AcOEt containing hydrogen chloride was putted into the obtained powder and agitated for 2 h, dried in vacuum, dissolved in acetonitrile/ Na_2CO_3 aqueous solution, added to FmocOSu, stirred for 6 h, acidified with $KHSO_4$ aqueous solution, and extracted with diethyl ether, and the organic phase was rinsed with brine and evaporated in vacuum. The resulting product was handled via column chromatography, and the Fmoc derivative **5** was obtained.

The PPP was synthesized in a similar method via the standard solid phase Fmoc-protocol on a peptide synthesizer (CEM, Matthews, North Carolina, USA) with the use of Nankai Hecheng Rink amide resin at a 0.44 mmol/g concentration (Tianjin, China).[19] The

crude peptides were purified using Waters PrepLC 4000 high-performance liquid chromatography with greater than 95% purity. MALDI-TOF-MS (Autoflex III; Bruker Daltonics Inc., Billerica, Massachusetts, USA) was employed to analysis the molecular weight of the obtained peptides.

Photo-triggered cleavage and zeta-potential of the PPP. To study the sensitivity of the PPP cleavage to NIR light, a solution of PPP in 50% v/v acetonitrile/phosphate buffer (pH 7.6, 20 mM) was illuminated with a NIR light (λ=740 nm, 0-50 $J \cdot cm^{-2}$, 0-83 mW, 2 min interval after 1 min irradiation), and the concentration of PPP at different time was measured using HPLC (Agilent 1211, Agilent Technologies, USA). The chromatographic conditions were as follows: a C_{18} column (250 mm×4.6 mm, 5 μm) (Agilent Technologies Inc., Avondale, PA, USA) and detection at 220 nm. To study the sensitivity of the pH, the zeta-potential of the PPP at pH 7.4 and 6.0 (with or without NIR illumination) was determined using a Marvin Zetasizer Nano analyser (Marvin Instruments Ltd., UK).

Synthesis of DSPE-PEG$_{2000}$-PPP. DSPE-PEG$_{2000}$-PPP and DSPE-PEG$_{2000}$-CPP were synthesized by conjugating DSPE-PEG$_{2000}$-Mal to the cysteine residue on PPP and CPP, respectively. DSPE-PEG$_{2000}$-CPP was one of the photoproducts of DSPE-PEG$_{2000}$-PPP, which was applied to indicate the penetrating capacity changes of DSPE-PEG$_{2000}$-PPP before and after the light activation. PPP and CPP were coupled with DSPE-PEG$_{2000}$-Mal (1:1 molar ratio) in chloroform that included triethylamine (TEA, 5 eq.) around 20 °C with stirring for 24 h. The resulting mix was putted in dialysis bag (its molecular weight cutoff was 3.5 kDa) with distilled water and dialyzed for 48 h to dispel the chloroform and unreacted materials. The liquid in dialysis bag was dried by a rotary evaporator and kept at -20 °C. The formation

of the conjugations was verified by a MALDI-TOF mass spectrometry (MALDI-TOF MS).

Preparation of the NPs. A double emulsion (w/o/w) technique was used to prepare the normal NPs (N-NPs) as described in a previous report.[20] Briefly, EGFR-siRNA (FAM-siRNA, NC-siRNA) and spermidine were added in Tris-EDTA buffer (10 mM Tris, 1 mM EDTA, pH 7.4) (TE buffer). After 30 min, the formed siRNA-spermidine complexes were dripping to a PLGA- (50 mg/ml) methylene chloride (DCM) solution at a volume ratio of 1:10 under a vortex. This mixture was emulsified via sonication using an ultrasonic processor (SCIENTZ-IID, Scientz Biotechnology Co., China) into the first emulsion (w/o). This emulsion was then poured into a Tris-EDTA buffered 5% (w/v) PVA (at a volume ratio of 1:3), which contained DSPE-PEG_{2000} as the conjugate to PLGA at a molar ratio of 1:100. The resultant mix was treated by ultrasound to generate the second emulsion (w/o/w). The emulsion was quickly putted into Tris-EDTA buffered 0.5 % (w/v) PVA at a volume ratio of 1:25, and the NPs were kept stirring for 4 h to evaporate the DCM and solidify the particles. To prepare the PPP-modified NPs (PPP-NPs), similar operations were carried out except the amount of DSPE-PEG_{2000}-PPPs, which were used to displace the equimolar lipids(5%, 10% and 20% molar ratio). The preparation of the CPP-modified NPs (CPP-NPs) followed the procedure of the PPP-NPs.

Characterization of NPs. Transmission electron microscopy (TEM, HITACHI, H-7650, Japan) and atomic force microscopy (AFM, NanoWizarc, JPK Ltd., Germany) were used to analysis the morphology of the prepared PPP-NPs. The diameter of the PPP-NPs was measured by a Marvin Zetasizer Nano analyzer (Marvin Instruments Ltd., UK). All assays were executed in triplicate.

Cellular uptake study. For flow cytometry, MCF-7 cells were cultured in 6-well culture plates overnight and each well contained 2×10^5 cells. After achieved 80-90% confluence, the cells were cultured in serum-free medium (pH of 7.4 or 6.0), which contained the different formulations including 75 nM FAM-siRNA. Among the samples, the PPP-NPs were pretreated with or without NIR illumination (λ=740 nm, 50 $J\cdot cm^{-2}$, 83 mW, 2 min interval after 1 min irradiation) for 30 min prior to their addition to the cells. After 4 h, the cells were digested with trypsin, rinsed with cold PBS, and then quickly analysed by a flow cytometry (BD FACSCalibur, USA). The mean fluorescence intensity is calculated by subtracting the fluorescence value of cells without any formulations.

For the confocal imaging, cells were seeded in 24-well culture plates with 2×10^5 cells each well. The following incubation operation was the same as above except that the FAM-siRNA of in every well was 225 nM. Afterwards, Hoechst 33258 was used to execute the nuclear staining (10 min). Then, the cells were analysed by a UltraVIEW Vox confocal laser scanning microscopy (CLSM) (UltraVIEW Vox, PerkinElmer, USA).

Evaluation of endosomal escape. After a 4 h cultivation with FAM-siRNA-loaded PPP-NPs (the samples were pretreated with NIR light illumination (λ=740 nm, 50 $J\cdot cm^{-2}$, 83 mW, 2 min interval after 1 min irradiation, total for 30 min) in the serum free medium under pH 6.0), MCF-7 cells were rinsed with cold PBS for three times and incubated in complete medium for an extra time (0.5 h or 2 h). LysoTracker Red (Invitrogen/Molecular Probes, CA, USA) was empoyed to executed the endosome/lysosome labeling for 0.5 h (500 nM). Thereafter, the cells were washed with cold PBS and assayed by the CLSM.

***In vitro* siRNA transfection and gene expression**. Small dishes (35-mm) were uesed to

culture the MCF-7 cells with 2.0×10^6 cells per well. After a 24 h incubation (37 °C with 5% CO_2), fresh and serum-free medium contained different siRNA-loaded NPs was used to replaced the former medium. Certain medium included with PPP-NPs (pH 7.4 or 6.0) would be irradiated with the NIR light (λ=740 nm, 50 $J\cdot cm^{-2}$, 83 mW, 2 min interval after 1 min irradiation, total for 30 min). After 5 h, the serum-free medium were removed and the complete medium were added for an extra 48 h (mRNA assays) or 72 h (protein quantification) in the incubator. After that, EGFR mRNA and its related proteins were respectively measured by a quantitative real-time polymerase chain reaction (qRT-PCR) and western blot analysis. The details of the two methods were described in our previous study.[21]

Cell apoptosis analysis. MCF-7 cells (2.0×10^6 per flask) in 6 mL of complete DMEM medium were plated on each tissue culture flask (25 cm^2). After a incubation of 24 h, the cells were rinsed with PBS (0.1 M, pH 7.4) and then added with serum-free medium including tested NPs. Certain medium included with PPP-NPs (pH 7.4 or 6.0) would be irradiated with the NIR light (λ=740 nm, 50 $J\cdot cm^{-2}$, 83 mW, 2 min interval after 1 min irradiation, total for 30 min). After a incubation of 6 h, the cells were gathered and handled with an Annexin V-FITC apoptosis detection kit (Beyotime Institute of Biotechnology, Jiangsu, China) based on the product's instructions, and were quickly measured by a FACScan flow cytometer (10,000 events per sample).

Animal model. Female BALB/c nude mice with the weight of 18-22 g were provided by Vital River Laboratories (Beijing, China). An xenotransplantation model was created by subcutaneously injecting MCF-7 cells as previously reported.[19] All treatments relating to the animals were authorized by the Animal Care and Use Ethics Committee of Beijing Institute

of Pharmacology and Toxicology.

***In vivo* distribution**. 200 μL of 5% glucose (control) and different formulations of NPs including Cy5-siRNA at 20 μg/kg were respectively injected to the MCF-7 tumor bearing nude mice by tail intravenous. After 4 h, the tumor-xenografted mice were fixed and the surfaces of the tumor sites (PPP-NPs group) was illuminated with the NIR light (λ=740 nm, 50 $J \cdot cm^{-2}$, 83 mW, 2 min interval after 1 min irradiation) at an exposure area of 1.0 cm^2 for 30 min. 6 h and 24 h after the injection, a IVIS® Lumina II *in vivo* imaging system (Caliper life sciences, USA) was used to obverse the fluorescence. After that, the animals were killed by anesthesia, and the tumor and major organs were removed and assayed.

***In vivo* antitumor efficacy**. The MCF-7 tumor-bearing nude mice were injected by tail intravenous with 5% glucose (control), free siRNA, and various formulations of NPs (20 μg/kg siRNA, corresponding to 1.2 mg/kg of NPs). The injection was performed once every other day for a total of 5 times. 4 h after the final injection, half of the mice in the PPP-NPs group were illuminated with the NIR light (λ=740 nm, 50 $J \cdot cm^{-2}$, 83 mW, 2 min interval after 1 min irradiation) for 30 min. The animals were weighed and their tumor volumes were metered by a Vernier caliper every day during the whole experiment period. The relative tumor volume (RTV) was computed as RTV = (tumor volume at day n)/(tumor volume at day 0)×100%.

Gene expression in tumor tissues. The *in vivo* EGFR expression analysis was performed 24 h after the final injection. The animals (n=3) were killed by anesthesia and their tumor were removed for analysis. Tumor pieces were obtained for the total mRNA (qRT-PCR) [22] or protein extraction (Western blot assay) [23] as described in the previous reports, respectively.

Immunohistochemical analysis. The apoptosis of the tumor tissues was performed 24 h after the final injection. The animals (n=3) were killed by anesthesia and their tumor were removed for analysis. For the immunohistochemical analysis, the obtained tumor tissues were first frozen and then cut into thin slices (4-mm). For apoptosis assay, TRITC staining in situ Apoptosis Detection Kit (KeyGEN, Nanjing, China) was used to performed the terminal deoxynucleotidyl transferase (TdT)-mediated dUTP nick end labeling (TUNEL) staining. The operation was carried out on the instructions of the kit. After the nuclei stained with PI (37 °C) for 25 min, the samples were then analysed by the CLSM.

Statistical analysis. Data were expressed as means ± standard deviation (SD). ANOVA analysis was used to calculate the difference between any two groups. The P value less than 0.05 was considered to be statistically significant.

■ RESULTS AND DISCUSSION

Synthesis and characterization of the PPP. The peptide was synthesized as shown in Fig. 2 A. Compound **1** was alkylated with photo-sensitive compound **2** in the presence of K_2CO_3 to generate compound **3**. Then, the TBS group of compound **3** was removed under the acidic condition, and PDC was added to oxidize the resulting hydroxyl group and afford compound **4**. After treatment with $NaClO_2$, acid treatment, and FmocOSu, the Fmoc-protected amino acid **5** was obtained. The total yield of the amino acid was approximately 70%. For the last step, amino acid **5** was incorporated into the designed peptide sequence via Fmoc solid-phase peptide synthesis (Fmoc SPPS). The observed mass of the PPP was 2976.03 Da (Fig. 2B, labeled with an arrow), which is equal to its theoretical molecular mass of 2975.49 Da.

The cleavage of the PPPs by NIR light stimulus is the critical stage to achieve the

dual-stimuli responsive PPP-NPs that were developed in this study. The 4, 5-dimethoxy-2-nitrobenzyl group is very sensitive to the 740 nm NIR irradiation, and it has been recently applied as a photo-cleavable group to govern the behaviours of cells.[24, 25] Due to its good stability and reactivity, this group was introduced into the linking moiety of a quasi amino acid. The NIR light would induce removal of the photo-cleavable group on the phenolic hydroxyl group [26] as displayed in Fig. 3A. When irradiated with the NIR laser, the photo-cleavable group would cleave, and then the pH-sensitive inhibitory peptide would dissociate from the polycationic CPP. CPP is the photochemical product of the PPPs, which was confirmed using an HPLC assay. After illumination, the PPPs (approximately 20 min) were converted to corresponding CPPs (approximately 11 min), as displayed in Fig. 3 B and C. These data suggest that the occurrence of a specific cleavage, as predicted. The rate of PPP cleavage was performed by the exposure of PPP solutions (in buffer) to NIR laser irradiation (Fig. 3D). The cleavage of PPP is related to the laser irradiation power. With an increase in irradiation power, there was an improvement in the degree of cleavage. When the irradiation power was 50 $J \cdot cm^{-2}$, approximately 92% and 94% of the initial chemical structure of PPP was split at 30 min and 60 min after the exposure, respectively, which was available for cell binding and penetration. Furthermore, the amount of the PPP did not decrease without NIR illumination. The PPP construct was highly susceptible to NIR light illumination, and thus, further experiments were performed using 50 $J \cdot cm^{-2}$ and 30 min of light illumination.

To enhance the separation efficiency, an inhibitory peptide (EEEERRRR) with an isoelectric point of 6.4 was designed and synthesized. This inhibitory peptide was pH-sensitive and it was negatively charged under physiological condition, but it would be

electrically neutral or even positively charged at a lower pHe. The corresponding zeta-potential values of the PPPs were 1.2 ± 3.1 mV at pH 7.4 (physiological condition) in the dark. Meanwhile, the zeta-potential values of the peptides were 5.5 ± 2.2 mV in the dark and 5.4 ± 1.9 mV after illumination at pH 6.0 (the mimetic tumor microenvironments). The pH-sensitive inhibitory peptide would be negatively charged under physiological conditions and thus cloak the CPP well, whereas this masking effect would be vanished in the tumor microenvironments.

Synthesis and identification of DSPE-PEG$_{2000}$-PPP. The PPP-NPs were developed by modifying the synthesized functional material, DSPE-PEG$_{2000}$-PPP. As shown in Fig. 4A, via the reaction between the cysteine residue and maleimide, the PPP was covalently conjugated to the terminus of DSPE-PEG$_{2000}$-Mal. DSPE-PEG$_{2000}$-PPP was successfully formed and this was verified by the results of MALDI-TOF MS. The synthesized products demonstrated a mass/charge ratio of 5893.01 (Fig. 4B, noted with an arrow), which is equal to the theoretical molecular mass of 5895.42. Additionally, DSPE-PEG$_{2000}$-CPP was the cleavage product of DSPE-PEG$_{2000}$-PPP. Here, DSPE-PEG$_{2000}$-CPP was also synthesized by the same method and was employed to measure the penetrating effect changes of DSPE-PEG$_{2000}$-PPP after its activation. The final product was then used to prepare targeted PPP-NPs or CPP-NPs in the experiments.

Preparation and characterization of the NPs. All of the functional materials that we used were pre-synthesized. Thus, these NPs (N-NPs, CPP-NPs and PPP-NPs) could be conveniently constructed via a single-step nanoprecipitation method.

Because the content of DSPE-PEG$_{2000}$-PPP in the NPs is a key factor that significantly

influences the cellular uptake efficiency of the NPs, the cellular uptake of different FAM-siRNA loading NPs with various amounts of DSPE-PEG$_{2000}$-PPP were evaluated in the MCF-7 cells to screen the formulations. As displayed in Fig. 5A, the cellular uptake of the prepared PPP-NPs was not changed in the dark by using various amounts of DSPE-PEG$_{2000}$-PPP. However, the cellular uptake of the PPP-NPs was remarkably affected by the addition of the DSPE-PEG$_{2000}$-PPP concentration after illumination. When the NPs were modified with 10% of DSPE-PEG$_{2000}$-PPP, the illumination would generate a notable increase of the cellular uptake. But when the DSPE-PEG$_{2000}$-PPP molar ratios continuously increased (20%), the uptake level decreased, which might suggest that a NIR light irradiation time of 30 min might be insufficient to photodegrade the added PPPs. Based on this, the preferred molar ratio of DSPE-PEG$_{2000}$-PPP on the NPs was chosen to be 10%. Additionally, the amount of DSPE-PEG$_{2000}$-CPP on the NPs was chosen to be 10% (molar ratio), and the CPP-NPs were also prepared using the same procedure.

The physiochemical characteristics of the three different NPs formulations are presented in Table 1. The siRNA encapsulation efficiency of all the three formulations was approximately 87%, and the siRNA in the PPP-NPs or PPP-NPs (with NIR) did not degrade much even after 24 h as showed in the Supporting Information. The particle size of the prepared NPs was in the range of 108 to 116 nm. This particle size was suitable for delivery in circulation. Because this size was large enough to avoid kidney filtration (>10 nm) but also small enough to cross over tissues, to approach cell surface receptors and aid the intracellular transport.[27] TEM and AFM observations confirmed the existence of the PPP-NPs (Fig. 5 B and C). The mean particle size of the PPP-NPs given by the TEM images was near the values

provided by the laser particle analyser (Fig. 5D). AFM was further used to describe the particle surface morphology of the PPP-NPs.

Table 1. Properties of the NPs (n = 3)

Sample ID	Dimater (nm)	Polydispersity index	Entrapment efficiency (%)
N-NPs	108.26 ± 0.11	0.10 ± 0.01	87.34 ± 2.02
CPP-NPs	113.68 ± 0.10	0.09 ± 0.01	86.87 ± 1.54
PPP-NPs	116.27 ± 0.12	0.10 ± 0.01	88.20 ± 1.92
PPP-NPs (NIR-pretreated)	115.56 ± 0.14	0.08 ± 0.01	87.05 ± 1.87

Cellular uptake and endosomal escape. In this experiment, flow cytometry and CLSM was used to analysis the cellular uptake of the tested NPs, in which FAM-siRNA was entrapped in as a fluorescent marker. As shown in Fig. 6A, compared with FAM-siRNA, the cellular uptake of CPP-NPs was remarkably increased, which could be due to the CPP-mediated translocation effect. Additionally, upon NIR light illumination at pH 6.0, the mean fluorescence intensity of the PPP-NPs (with NIR, under pH 6.0) was 115.73, which was at a similar level to the CPP-NPs, suggesting that the PPPs were surffiently revitalized to execute CPP's penetrating effect on the mimetic tumor. Meanwhile, at pH 7.4, the mean fluorescence intensity of the PPP-NPs (with NIR at pH 7.4) declined to 92.42 even when pretreated with NIR to cleave the linker, which could be explained by the insufficient separation of the pH-sensitive inhibitory peptide with the CPP segment after cleavage. On the contrary, the mean fluorescence intensity of the PPP-NPs (without NIR light) was not ideal,

either at pH 7.4 (42.55) or 6.0 (44.87), they were similar as that of N-NPs (41.35). The results suggest that the photo-cleavable group was not cleaved without the NIR irradiation. The CPP was still shielded by the pH-sensitive inhibitory peptide, and the penetrating ability of the PPP was not activated even at pH 6.0. All of these results indicate that both NIR light and a low pH are indispensable to activating PPP. From the CLMS results, simiar trend was found in the cellular uptake experiment. As displayed in Fig. 6B, the N-NPs and PPP-NPs (without NIR) groups had a alike relatively low cellular uptake, either at pH 7.4 or 6.0. Whereas, the CPP-NPs had a remarkble cellular uptake. After the treatment of NIR irradiation, compared with the PPP-NPs (with NIR at pH 7.4), the PPP-NPs (with NIR at pH 6.0) showed a remarkble increase of cellular uptake, implying the activation of PPP. This result might be due to the synergism between the photo activation and pH sensitiveness. The above results are consistent with that of flow cytometry analysis. Overall, the above cell uptake data intensily support our previous anticipation, PPPs combined with NIR light, can enhance the cancer cells recognition and uptake of prepared carriers, and thus reduce the nonspecific cell uptake.

After internalization by the cells via the activated CPP, the ability of the siRNA-loaded PPP-NPs to surmount over the intracellular endolysosomal delivery barriers and efficiently deliver siRNA into the cytoplasm is crucial for the efficient gene silencing activities of siRNA. FAM-siRNA that was formulated in the PPP-NPs (with NIR at pH 6.0) and then incubated with cells stained with LysoTracker (red) to track endosomal escape by CLSM. As shown in Fig. 6C, for the FAM-siRNA-loaded PPP-NPs (with NIR at pH 6.0), the endosomal escape is time-dependent within 0.5 h of transfection, and the yellow fluorescence in the

figure suggests the colocalization of the green fluorescent FAM-siRNA and the LysoTracker Red-labelled endosomes/lysosomes. After transfecting for 2 h, most green fluorescence was found in the cytosol but not coexisted with LysoTracker (red), suggested that much FAM-siRNA was left from the lysosomes and come into the cytoplasm. This phenomenon could be explained as follows: the sequence of CCP (positively charged) can assemble ion pairs with the lipids (negatively charged) in endosome membrane and therefore replace the surface-bound water on endosome membrane, and consequently break the endosomal membrane.[28]

***In vitro* gene silencing and cell apoptosis assay**. The *in vitro* gene silencing activity of EGFR-siRNA against the EGFR gene that was delivered by the PPP-NPs was further determined using qRT-PCR and western blot analysis. As exhibited in Fig. 7 A and B, the EGFR mRNA and protein expression of the MCF-7 cells incubated with NC-siRNA-loaded PPP-NPs (with NIR, under pH 6.0) were not inhibited, while the cells treated to different NPs loaded with EGFR-siRNA displayed a decreased EGFR gene expression, suggesting a gene silencing. However, the results display that free EGFR-siRNA does not exhibit gene silence activity for EGFR, indicating that free siRNA cannot easily cross the cell membrane for their negative charge and large volume.[29] Among all the groups, the PPP-NPs and CPP-NPs groups in MCF-7 cells showed the stronger silencing effect, which is also agreed with the cell uptake results (Fig. 6 A and B). Compared with the no NIR irradiated PPP-NPs group (pH 6.0), NIR irradiated PPP-NPs (pH 6.0) group showed lowered EGFR mRNA and protein expressions. This indicated that the NIR irradiation could increase cell uptake of siRNA by the photo-degradation of PPPs. Additionally, the PPP-NPs (with NIR at pH 6.0)

demonstrated stronger gene silencing effect than the PPP-NPs (with NIR, under pH 7.4), which could be due to the increased internalization of EGFR-siRNA. This suggests an adequately activated PPP-mediated cell uptake of carriers with PPP modification, as exhibited in the cellular uptake experiment (Fig. 6 A and B).

In the treated MCF-7 cells, apoptosis, which was induced by various formulations that carried NC-siRNA and EGFR-siRNA, were analysed via a flow cytometry. The MCF-7 cells that were exposed to the EGFR-siRNA loaded formulations showed significant apoptosis (33%-67%), suggesting that the apoptosis was primarily yielded from the low expression of EGFR. Additionally, the delivery of the EGFR-siRNA-loaded PPP-NPs (with NIR, under pH 7.4) (48%) produced a higher level of apoptosis than that of N-NPs (33%), PPP-NPs (without NIR, under pH 6.0) (32%) and PPP-NPs (without NIR, under pH 7.4) (34%). As expected, compared with the PPP-NPs (with NIR, under pH 7.4), cells exposed to the PPP-NPs (with NIR, under pH 6.0) that were loaded with EGFR-siRNA presented a higher percentage (59%) of apoptotic cells, which is in accordance with the aforementioned mRNA and protein expression analysis results (Fig. 7 A and B). Whereas, a weak cell apoptosis was found in the control and NC-siRNA-loaded PPP-NP (with NIR at pH 6.0) groups (3%), implying that the HT-1080 cells' apoptosis were also generated from the down regulation of EGFR mRNA. Among all of the tested formulations, the CPP-NPs containing EGFR-siRNA demonstrated the most significant apoptosis at 67%.

Therefore, these results demonstrate that the PPP ligand that was introduced into the NPs significantly helped the RNAi induced gene silencing and growth inhibition, when the PPPs were split by the NIR irradiation to form dissociative CPPs by the lowered pHe.

***In vivo* imaging**. The *in vivo* distribution and tumor-targeting characteristics of the payload formulated in the NPs was investigated in a MCF-7 nude mice model by using Cy5-siRNA. For NIR imaging, illumination of a cyanine dye was not exactly at the absorption wavelength, this may cause some loss of fluorescence due to photo-bleaching. As shown in Fig. 8A, in the mice treated with PBS, no fluorescence was observed during the experimental period. As the fluorescence intensity of free Cy5-siRNA rapidly decreased after intravenous injection, tumor accumulation did not occur. The reason for this phenomenon is related with the inherent problems of siRNA, such as its instant degradation by Rnase (A type of nucleases) and its rapid renal excretion after administration. After illumination, the PPP-NP (with NIR)-treated mice exhibited the most intense tumor distribution during the entire period. Moreover, the result was further verified by the strongest fluorescence signals found in the isolated tumor tissues (Fig. 8B). This accordance indicated that the nanocarriers modified with PPPs could enhance their accumulation in the tumors, which benefited from the dual stimuli of the NIR light illumination and lowered pHe. In contrast, for the CPP-NP group, fluorescence signal from the tumor site almost disappeared after 24 h. Due to the no specific cell penetrating ability of CPP, the CPP-NPs had a lower *in vivo* tumor selectivity than the PPP-NPs (with NIR). However, the higher cellular uptake of FAM-siRNA in the CPP-NP group (Fig. 6 A and B) could be attributed to the assisted entry of the NPs into the cells via CPP. For the N-NPs, the fluorescence in the tumor sits lasted for 24 h but its intensity was notably decreased. The non-modified NPs provided an impressive selective-drug-transport via the EPR effect,[30] which is due to the suitable particle size of the NPs. Additionally, the mice injected with the PPP-NPs (without NIR) exhibited a lower

fluorescence intensity in the tumor similar to the N-NPs, suggesting the cancer cells were recognized and the penetrating ability of the PPPs was not activated. Although the electrostatic attraction of the CPP and the pH-sensitive inhibitory peptide was eliminated at the *in vivo* lowered pHe, the photo-cleavable group was not cleaved without NIR light illumination, and the CPP was still shielded by the pH-sensitive inhibitory peptide.

The isolated organs and tumor tissues were further observed by sacrificing the mice 24 h after administration. As shown in Fig. 8B, the tumors from the PPP-NP (with NIR)-treated group displayed the strongest fluorescence signals, whereas less fluorescence was observed in other organs. The results suggest that the PPP-NPs (with NIR) can efficiently and selectively delivery the siRNA to the tumor sites of nude mice model, and thus reduce the non-specific cumulation in the healthy tissues. Meanwhile, the PPP-NP (with NIR)-treated group exhibited a comparable fluorescence intensity in liver and kidneys, which is consistent with another recent study.[31] This demonstrates that nanocarriers may target tumors to some extent via PPP mediation. Meanwhile, the nanocarriers could also be subject to reticuloendothelial system (RES) uptake and renal excretion. However, the related strong liver and kidney uptake mechanisms of the PPP-mediated nanocarriers *in vivo* require further study.

Overall, these results demonstrated that the PPP-NPs (with NIR) have the latent capacity to realize the selective delivery of siRNA to a tumor *in vivo*.

***In vivo* antitumor efficacy**. Inspired by the satisfactory tumor target results, we further explored the *in vivo* antitumor activity of the PPP-NPs that carry EGFR-siRNA in MCF-7 xenografted nude mice.

According to the results of the preliminary experiment, the max fluorescence would

appear in the tumor sit about 4 h after the injection, which indicated that there would be a great of nanoparticles accumulated in the tumor 4 h after the administration. Therefore, to gain a high siRNA concentration in the tumor site, the irradiation was operated at 4 h after the injection. This point in time for light illumination was near to Park et al. reported (6 h)[32]. The irradiation power was selected by the *in vitro* results (Figure 3D). The irradiation time was mainly chosen based on the thermo influence of the light. To avoid the NIR light to burn the exposed tumor tissue, 30 min exposure (2 min interval after 1 min irradiation) was chosen. Because at this time setting (under 50 $J \cdot cm^{-1}$), only a slight increase of the tumor temperature was observed (less than 1 °C).

As shown in Fig. 9A, due to the inherent shortfalls of siRNA, mice in the free EGFR-siRNA groups (RTV = 543 ± 44%) exhibited no significant tumor growth inhibition compared to the glucose group (RTV = 571 ± 42%) at day 18, which displayed almost no growth inhibition. Additionally, the administration of NC-siRNA-contained PPP-NPs (with NIR, RTV = 531 ± 41%) showed no tumor inhibition effect, suggesting that the anticancer activity of NPs that carried siRNA was specially associated with EGFR-siRNA. However, compared to the control group, the groups contained EGFR-siRNA as N-NPs (RTV = 349 ± 41%) and PPP-NPs (without NIR, RTV = 333 ± 58%) exhibited a mild increase of tumor inhibition effect. These results demonstrated that the introducing of EGFR-siRNA into the nanocarrier could improve the *in vivo* tumor inhibition effect. However, as expected, the PPP-NP (with NIR) group containing with EGFR-siRNA (RTV = 235 ± 49%) displayed a superior antitumor effect. A reason for this may be the improved EGFR-siRNA transfection efficiency by PPP-NPs (with NIR) with the dual stimulus of photons and pH. This result was

consistent with the aforesaid results, which revealed the superiority of PPP-NPs (with NIR) than the other tested nanocarriers evaluated in *in vivo* imaging (Fig. 8 A and B). In contrast, for the EGFR-siRNA-loaded CPP-NP-treated group (RTV = 411 ± 40%), which was attributed to the CPPs' non-selective penetrating ability.[33] The modification of the nanocarrier surfaces with CPPs leads to a specific interaction and uptake in non-targeted cells. This drawback limits the *in vivo* antitumor efficacy of CPP-NPs. With respect to evaluation of the safety, the body weight of the tumor-bearing mice was recorded through the testing period. As shown in Fig. 9B, there was no remarkable body weight changes among the tested groups during the whole experiment, indicating the safety of our formulations.

To test whether the antitumor effect (as displayed above) was related to the EGFR gene silencing, the mRNA and protein levels of EGFR in tumors was respectively evaluated using qRT-PCR and western blot analysis, after sacrificing the animals at the completion of the study. For the PPP-NPs containing EGFR-siRNA (with NIR), both the EGFR mRNA (Fig. 9C) and the protein (Fig. 9D) levels exhibited obvious alterations compared with other formulations. The results of molecular analysis were in coincidence with the antitumor effects previously described (Fig. 9A), providing the proofs for the correlation between the tumor inhibition and EGFR gene silencing.

Terminal deoxynucleotidyl transferase (TdT)-mediated dUTP nick end labeling (TUNEL) technique was widely applied in the estimate of tumor cell apoptosis via detecting the breaks in DNA strand.[34] As shown in Fig. 9E, neither control (5% glucose) nor free siRNA groups displayed no green fluorescence (usually appeared in TUNEL-positive cells), indicating no remarkable cell apoptosis was detected. In contrast, the EGFR-siRNA-loaded

PPP-NPs (with NIR) group demonstrated remarkable cell apoptosis (with stronger green fluorescence) as compared with the other groups containing siRNAs. This pattern found in the apoptotic experiment was in coincidence with the results exhibited in the study of *in vivo* antitumor efficacy.

Therefore, the aforementioned results suggested that the anti-tumor effect of the EGFR-siRNA-entrapped PPP-NPs combined with NIR irradiation is remarkably better than that of free and other NPs in the nude mice tumor models, indicating the combined mechanisms of photon and pH activation. However, the restraint of the NIR light method is that the used external stimulus is limited to the surface tissues, notwithstanding a deep organization may be approached via the aid of laparoscopy in the clinic. As a proof of principle study, the long term toxicity effects of the prepared NPs was not studied in this report, and this test will be performed when the NPs are pushed into the new drug research process.

■ CONCLUSION

Here, we presented an effective dual-stimuli responsive nanoparticle system, PPP-NPs, which can efficiently transport entire siRNA into the target cells for *in vivo* siRNA transfection. After intravenous injection, the PPP-NPs can cumulate at the tumor sites through the EPR effect, and then they will penetrate into the target cells via the activation of CPP, which is triggered by NIR light illumination at the tumor site and lowered the pHe. Although in preliminary, this study provided a novel strategy for experimental and clinical oncotherapy and encourages further investigations in the exploration of CPPs.

SUPPORTING INFORMATION

The siRNA encapsulation efficiency (EE) of prepared formulations (1) and stability of siRNA-loaded NPs (2).

■ ACKNOWLEDGMENTS

The authors gratefully acknowledge funding from the National Natural Science Foundation of China (Grant No. 81202466 and 81402874) and the Important National Science & Technology Specific Projects (Grant No. 2012ZX09301003-001-009) of China, which supported this research.

■ REFERENCES

(1) Vive`s, E. Present and future of cell-penetrating peptide mediated delivery systems: ‘‘is the Trojan horse to wild to go only to Troy?’’. *J. Control. Release.* **2005,** *109*, 77-85.

(2) Jiang, T; Olson, E. S.; Nguyen, Q. T.; Roy. M.; Jennings, P. A.; Tsien, R. Y. Tumor Imaging by Means of proteolytic activation of cell-penetrating peptides. *Proc. Natl. Acad.Sci. U.S.A*. **2004,** *101*, 17867-17872.

(3) Shi, N. Q.; Gao, W.; Bai, X.; Qi, X. R. Ehancing cellular uptake of activable cell-penetrating peptide-doxorubicin conjugate by enzymatic cleavage. *Int. J. Nanomedinine.* **2012**, *7*, 1613-1621.

(4) Koren, E.; Torchilin, V. P. Cell-penetrating peptides: breaking through to the other side. *Trends Mol. Med*. **2012**, *18*, 385-393.

(5) Jiang, T.; Zhang, Z.; Zhang, Y.; Lv, H.; Zhou, J.; Li, C.; Hou, L.; Zhang, Q. Dual-functional liposomes based on pH-responsive cell-penetrating peptide and

hyaluronic acid for tumor-targeted anticancer drug delivery. *Biomaterials.* **2012**, *33*, 9246-9258.

(6) Krate, F.; Abu Ajaj, K.; Warnecke, A. Anticancer carrier-linked prodrugs in clinincal trials. *Expert Opin. Investig. Drugs.* **2007**, *16*, 1037-1058.

(7) Li, L.; ten Hagen T. L.; Schipper, D.; Wijnberg T. M.; van Rhoon, G. C.; Eggermont, A.M.; Lindner, L.H.; Koning, G.A. Triggered content release from optimizedstealth thermosensitive liposomes using mild hyperthermia. *J. Control. Release.* **2010**, *143*, 274-279.

(8) Hambley, T. W. Is anticancer drug development heading in the right direction? *Cancer Res.* **2009,** *69*, 1259-1261.

(9) Zhang, J.; Chen, H. Y.; Xu, L.; Gu, Y. Q. The targeted behavior of thermally responsivenanohydrogel evaluated by NIR system in mouse model. *J. Control. Release.* **2008**, *131*, 34-40.

(10) Melancon, M. P.; Elliott, A. M.; Shetty, A.; Huang, Q.; Stafford, R.J.; Li, C.; Near-infrared light modulated photothermal effect increases vascular perfusion and enhances polymeric drug delivery. *J. Control. Release.* **2011**, *156*, 265-272.

(11) Shigenaga, A.; Yamamoto, J.; Sumikawa, Y.; Furuta, T.; Otaka, A. Development and photo-responsive peptide bond cleavage reaction of two-photon near-infrared excitation-responsive peptide. *Tetrahedron. Lett*. **2010**, *51*, 2868-2871.

(12) Huang, S.; Shao, K.; Kuang, Y.; Liu, Y.; Li, J.; An, S.; Guo, Y.; Ma, H.; He, X.; Jiang, C. Tumor targeting and microenvironment-responsive nanoparticles for gene delivery. *Biomaterials.* **2013**, *34*, 5294-5302.

(13) Huang, S.; Shao, K.; Liu, Y.; Kuang, Y.; Li, J.; An, S.; Guo, Y.; Ma, H.; Jiang, C. Tumor targeting and microenvironment-responsive smart nanoparticles for combination therapy of antiangiogenesis and apoptosis. *Acs. Nano.* **2013**, 7, 2860-2871.

(14) Lee, E. S.; Gao, Z.; Bae, Y. H. Recent progress in tumor pH targeting nanotechnology. *J. Control. Release.* **2008**, *132*, 164-170.

(15) Zhang, X. M.; Lin, Y. X.; Gillies, R. J. Tumor pH and its measurement. *J. Nucl. Med.* **2010**, *51*, 1167-1170.

(16) Fischer, P. M.; Zhelev, N. Z.; Wang, S.; Melville, J. E.; Fahraeus, R.; Lane, D.P. Structure-activity relationship of truncated and substituted analogues of the intracellular delivery vector Penetratin. *J. Pept. Res.* **2000**, *55*, 163-172.

(17) Kim, D. H.; Rossi, J. J. Strategies for silencing human disease using RNA interference. *Nat. Rev. Genet*. **2007**, *8*, 173-184.

(18) Yang, Y.; Xie, X.; Yang, Y.; Zhang, H.; Mei, X. Photo-responsive and NGR-mediated multifunctional nanostructured lipid carrier for tumor-specific therapy. *J. Pharm. Sci*. **2015**, *104*, 1328-1339.

(19) Yang, Y.; Yang, Y.; Xie, X.; Wang, Z.; Gong, W.; Zhang, H.; Li, Y.; Yu, F.; Li, Z.; Mei, X. Dual-modified liposomes with a two-photon-sensitive cell penetrating peptide and NGR ligand for siRNA targeting delivery. *Biomaterials.* **2015**, *48*, 84-96.

(20) Cun, D.; Foged, C.; Yang, M.; Frokjar, S.; Nielsen, H. M. Preparation and characterization of poly (DL-lactide-co-glycolide) nanoparticles for siRNA delivery. *Int. J. Pharm*. **2010**, *390*, 70-75.

(21) Xie, X.; Yang, Y.; Yang, Y.; Mei, X. Photolabile-caged peptide-conjugated liposomes for

siRNA delivery. *J. Drug. Target*. **2015**, *23*, 789-799.

(22) Xiang, B.; Dong, D.W.; Shi, N. Q.; Gao, W.; Yang, Z. Z.; Cui, Y.; Cao, D. Y.; Qi, X. R. PSA-responsive and PSMA-mediated multifunctional liposomes for targeted therapy of prostate cancer. *Biomaterials.* **2013**, *34*, 6976-6991.

(23) Zhao, Z. X.; Gao, S. Y.; Wang, J. C.; Chen, C. J.; Zhao, E. Y.; Hou, W. J.; Feng, Q.; Gao, L. Y.; Liu, X. Y.; Zhang, L. R.; Zhang, Q. Self-assembly nanomicelles based on cationic mPEG-PLA-*b*-Polyarginine (R_{15}) triblock copolymer for siRNA delivery. *Biomaterials.* **2012**, *33*, 6793-6807.

(24) Neveu, P.; Aujard, L.; Benbrahim, C.; Saux, T. L.; Allemand, J. F.; Vriz, S.; Bensimon, D.; Jullien, L. A caged retinoic acid for one- and two-photon excitation in zebrafish embryos. *Angew. Chem. Int. Ed*. **2008**, *47*, 3744-3746.

(25) Dakin, K.; Li, W.H. Cell membrane permeable esters of D-myo-inositol 1,4,5-trisphosphate. *Cell. Calcium.* **2007**, *42*, 291-301.

(26) Jung, M. E.; Piizzi, G. Gem-disubstituent effect: theoretical basis and synthetic applications. *Chem. Rev*. **2005**, *105*, 1735-1766.

(27) Allen, T. M.; Hansen, C.; Martin, F.; Redemann, C.; Yau-Young, A. Liposomes containing synthetic lipid derivatives of poly (ethylene glycol) show prolonged circulation half-lives *in vivo*. *Biochim. Biophys. Acta.* **1991**, *1066*, 29-36.

(28) Morris, M. C.; Chaloin, L.; Méry, J.; Heitz, F.; Divita, G. A novel potent strategy for gene delivery using a single peptide vector as a carrier. *Nucleic. Acids. Res*. **1999**, 27, 3510-3517.

(29) Davis, M. E.; Zuckerman, J. E.; Choi, C. H.; Seligson, D.; Tolcher, A.; Alabi, C. A.; Yen,

Y.; Heidel, J. D.; Ribas, A. Evidence of RNAi in humans from systemically administered siRNA via targeted nanoparticles. *Nature.* **2011**, *464*, 1067-1070.

(30) Fang, J.; Nakamura, H.; Maeda, H. The EPR effect: unique featuresof tumor blood vessels for drug delivery, factors involved, and limitations and augmentation of the effect. *Adv. Drug. Deliv. Rev.* **2011**, *63*, 136-151.

(31) Huang, Y.; Lin, D.; Jiang, Q.; Zhang, W.; Guo, S.; Xiao, P.; Zhang, S.; Wang, X.; Chen, H.; Zhang, H. Y.; Deng, L.; Xing, J.; Du, Q.; Dong, A.; Liang, Z. Binary and ternary complexes based on polycaprolactone-graft-poly (N, N-dimethylaminoethyl methacrylate) for targeted siRNA delivery. *Biomaterials.* **2012**, *33*, 4653-4664.

(32) Park SJ.; Park W.; Na K. Photo-activatable ternary complex based on a multifunctional shielding material for targeted shRNA delivery in cancer treatment. *Biomaterials*. **2013**, *34*, 8991-8999.

(33) Huang, Y.; Jiang, Y.; Wang, H.; Wang, J.; Shin, M. C.; Byun, Y.; He, H.; Liang, Y.; Yang, V. C. Curb challenges of the "Trojan Horse" approach: Smart strategies in achieving effective yet safe cell-penetrating peptide-based drug delivery. *Adv. Drug. Deliv. Rev.* **2013**, *65*, 1299-1315.

(34) Yang, X. Z.; Dou, S.; Wang, Y. C.; Long, H. Y.; Xiong, M. H.; Mao, C. Q.; Yao, Y. D.; Wang, J. Single-step assembly of cationic lipid-polymer hybrid nanoparticles for systemic delivery of siRNA. *ACS. Nano*. **2012**, *6*, 4955-4965.

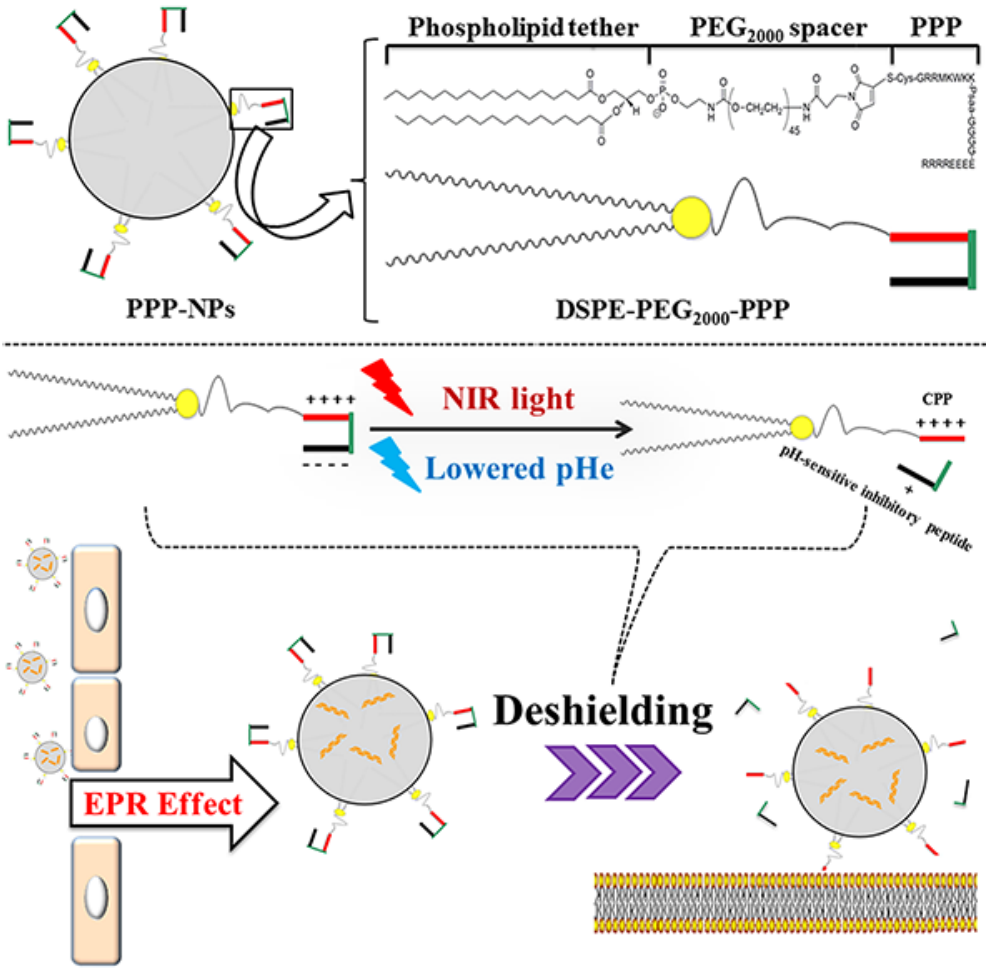

Upon NIR light illumination, the photo-cleavable group is cleaved. Simultaneously, the pH-sensitive inhibitory peptide eliminates the electrostatic attraction at a lowered pHe. Then, the activated NPs rapidly enter the cells.

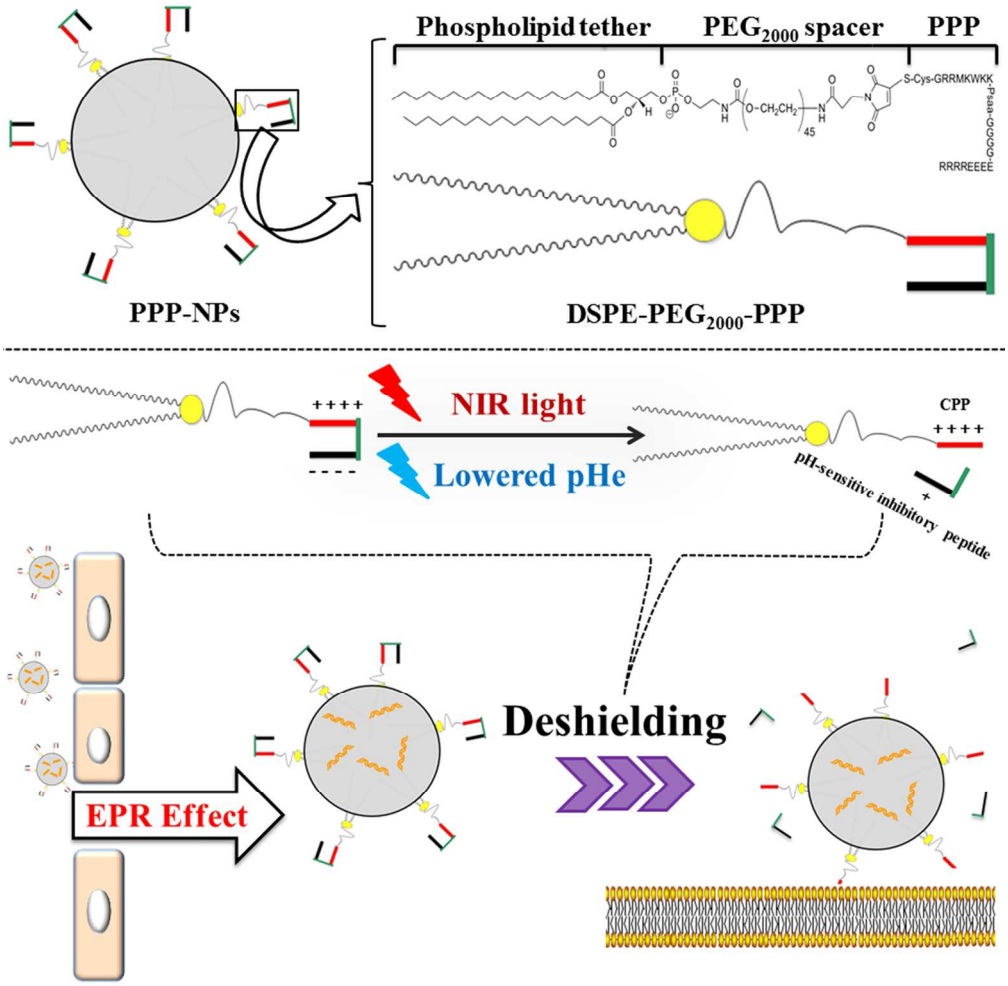

Captions

Figure 1. Schematic illustration of the PPP-NPs. The siRNA-loaded NPs are comprised of a spherical PLGA core that is coated with a phospholipid-linked PEGylated photo- and pH-responsive polypeptide (PPP) ligand.
148x147mm (300 x 300 DPI)

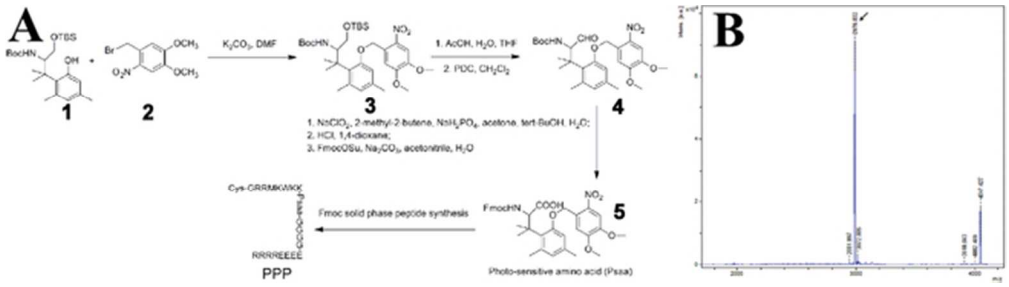

Figure 2. Synthetic procedure for the PPPs (A). MALDI-TOF mass spectra of the PPPs (B).
27x7mm (600 x 600 DPI)

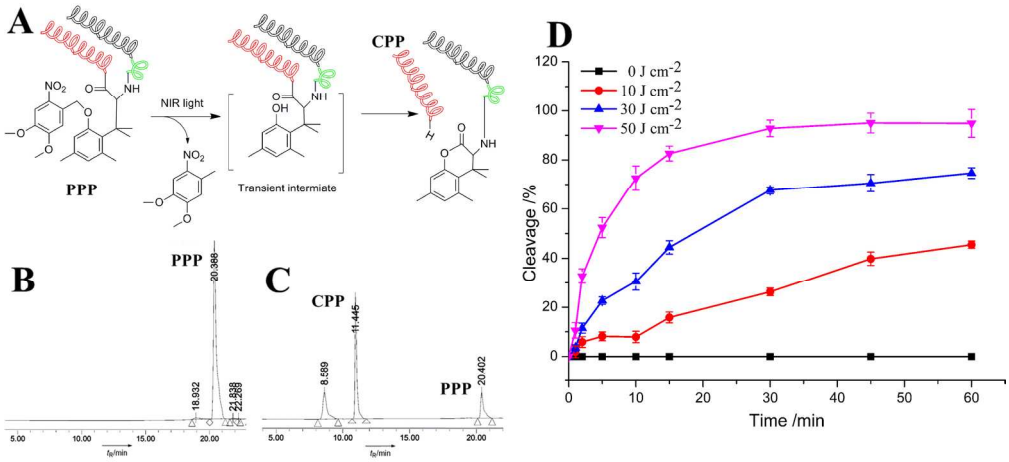

Figure 3. Principle of the NIR irradiation reaction of the PCPP (A). HPLC profiles before (B) and after (C) NIR irradiation. HPLC analysis of the cleavage of the PPPs via NIR irradiation (D). The responses of the PPPs are plotted versus time following the illumination with NIR light or after darkness at 37 °C.
92x42mm (600 x 600 DPI)

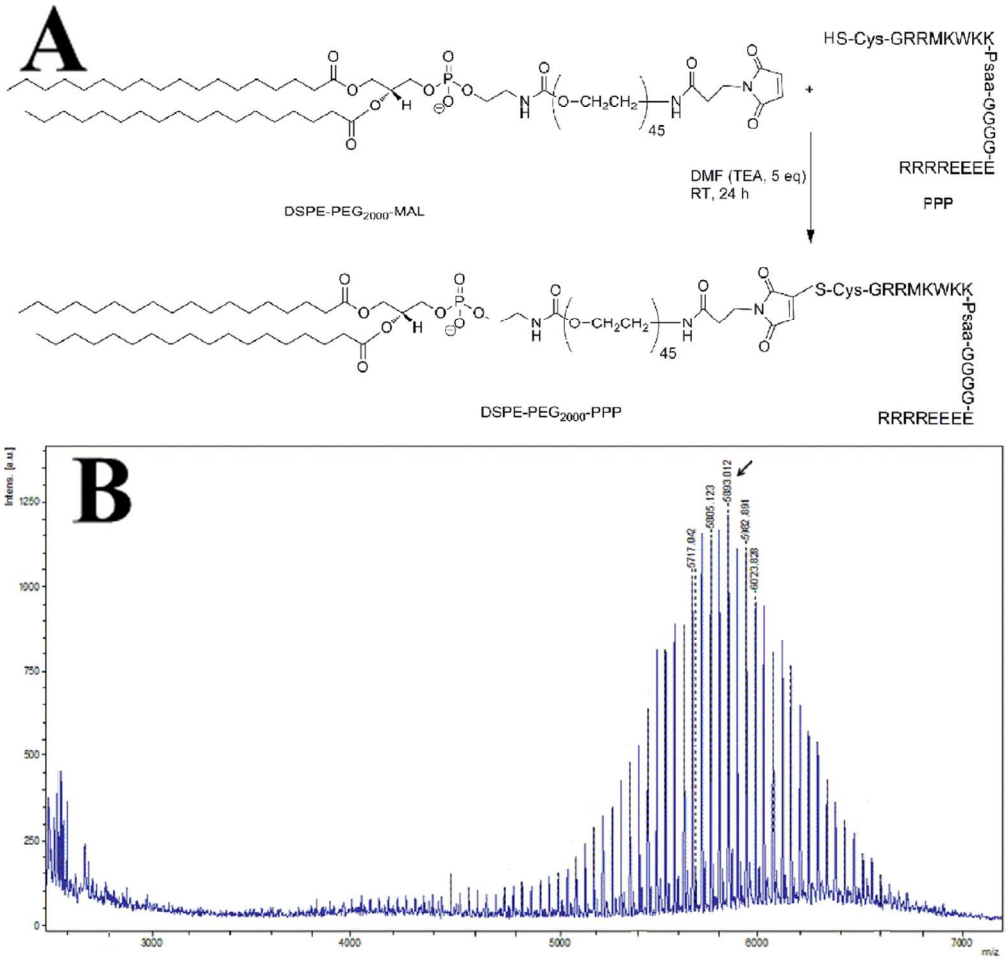

Figure 4. Synthesis method for DSPE-PEG2000-PPP (A). MALDI-TOF mass spectra of DSPE-PEG2000- PPP (B).
57x55mm (600 x 600 DPI)

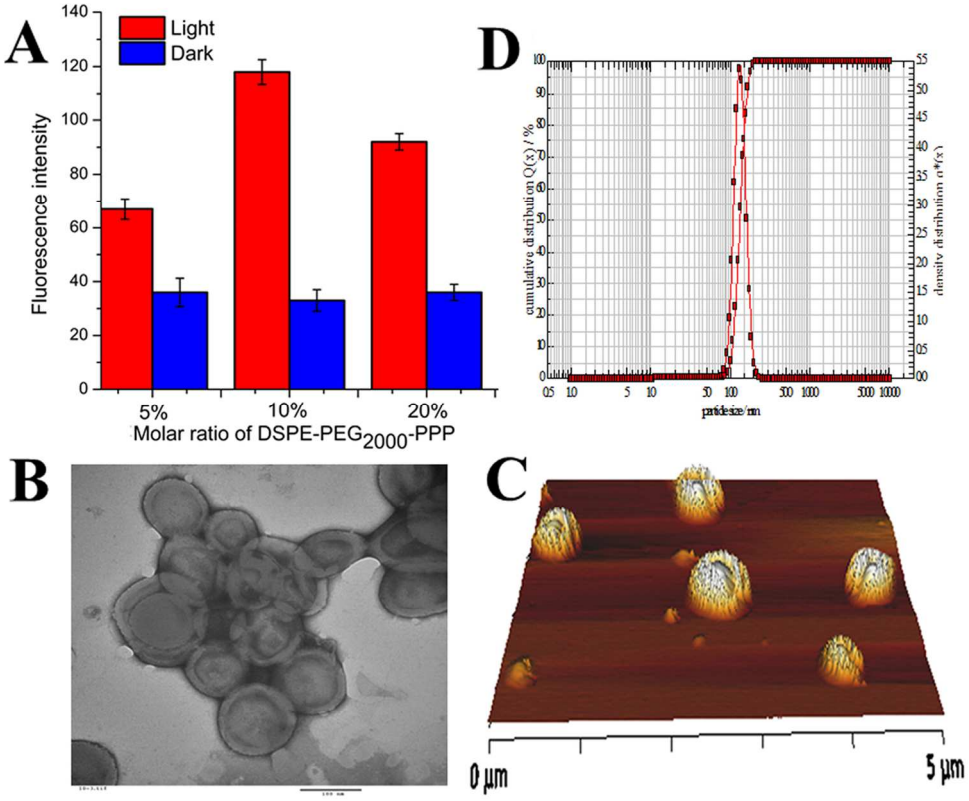

Figure 5. Physiochemical characterization of the PPP-NPs. The cellular uptake of different formulations of PPP-NPs by the MCF-7 cells (A). Morphological appearance of the PPP-NPs based on TEM (B) and AFM (C). Particle size distribution of the PPP-NPs (D). The data are presented as the means ± SD (n = 3).
64x52mm (600 x 600 DPI)

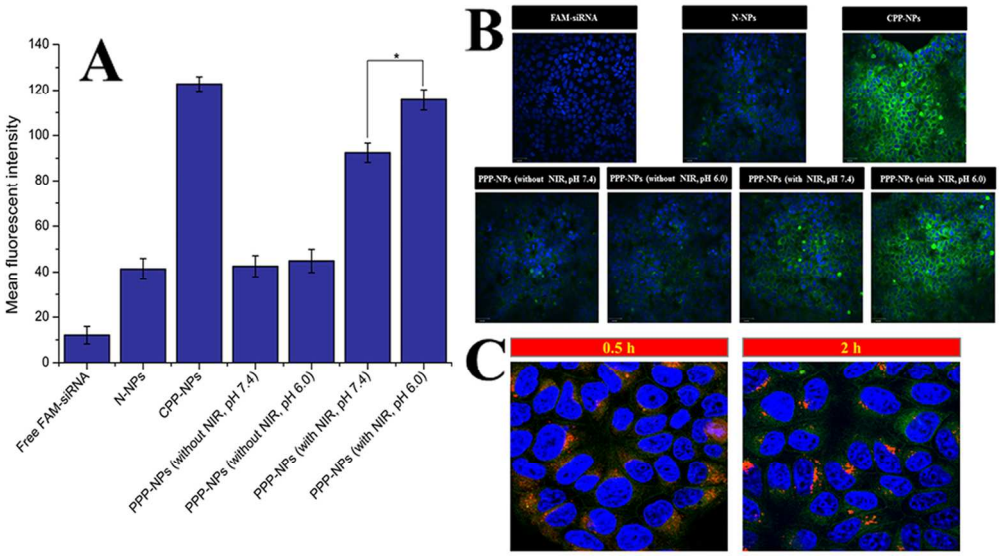

Figure 6. Cellular uptake of the PPP-NPs into the MCF-7 cells (A). Confocal laser scanning microscopy (CLSM) analysis of the uptake of various samples by the MCF-7 cells (B). Intracellular trafficking of the FAM-siRNA in the MCF-7 cells undergoing 0.5 h or 2 h of routine culture after 4 h of incubation with the NIR-pretreated PPP-NPs (C). Hoechst 33258 for nuclei staining (blue), FAM-siRNA fluorescence (green) and LysoTracker Red for the endosomes/lysosomes (red) were recorded. The data are presented as the means ± SD (n = 3). * indicates P< 0.05.
55x30mm (600 x 600 DPI)

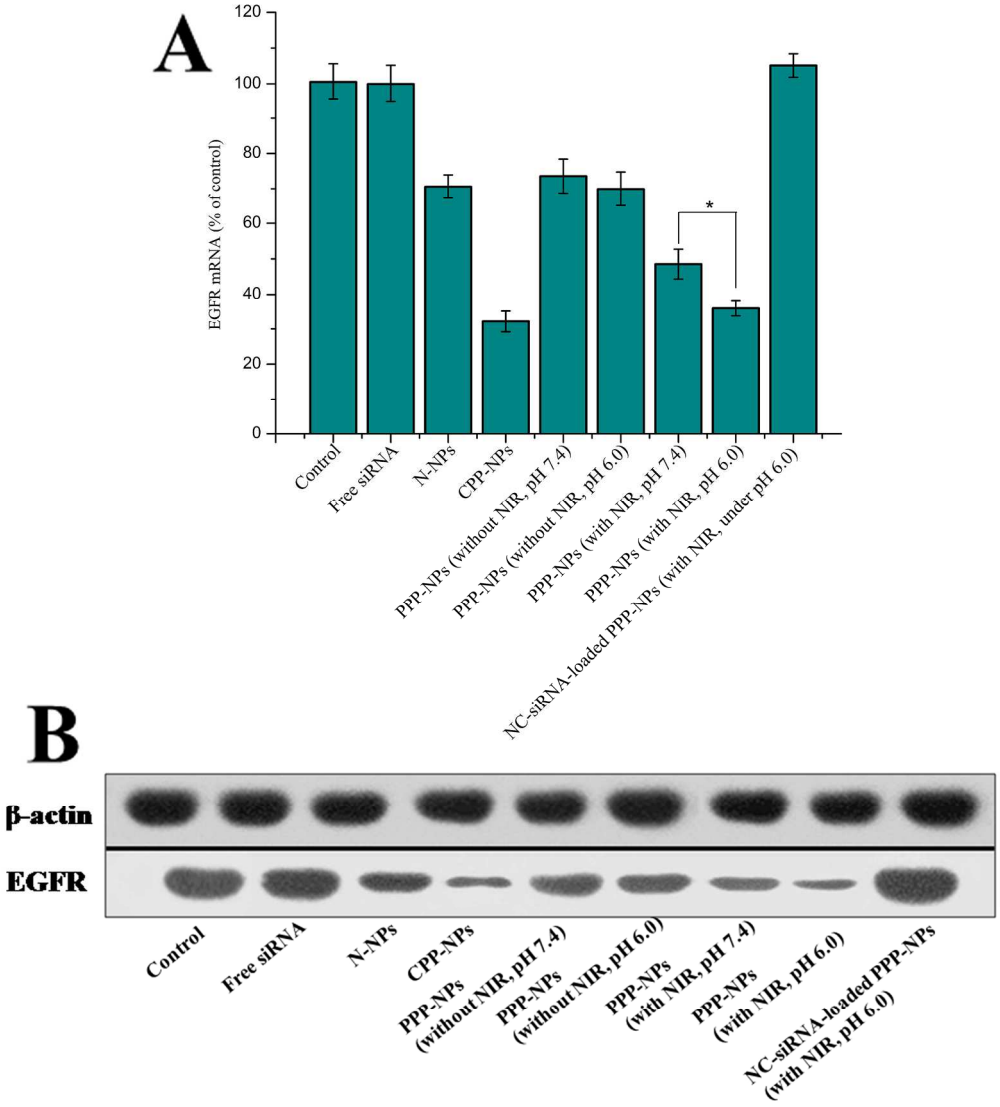

Figure 7. The level of EGFR mRNA, as determined by qRT-PCR (A). EGFR protein expression, as determined by western blot analysis (B). The data are presented as the means ± SD (n = 3). *indicates P< 0.05.
133x148mm (600 x 600 DPI)

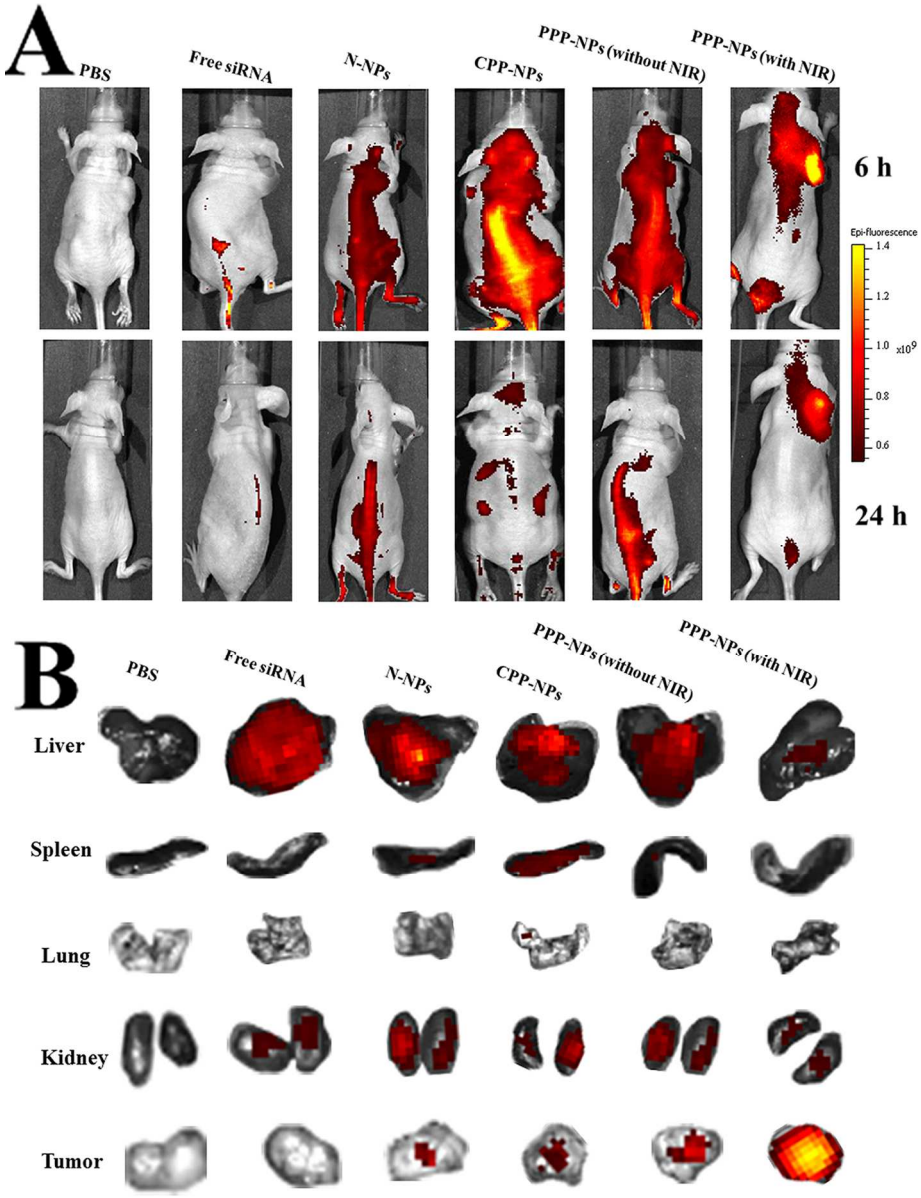

Figure 8. Biodistribution of Cy5-siRNA that was contained in various liposomes in mice bearing MCF-7 tumour xenografts. Whole body images at different times after systemic administration (A). Fluorescence detection of isolated main tissues and organs from mice at the end of the observation time (B).
150x195mm (300 x 300 DPI)

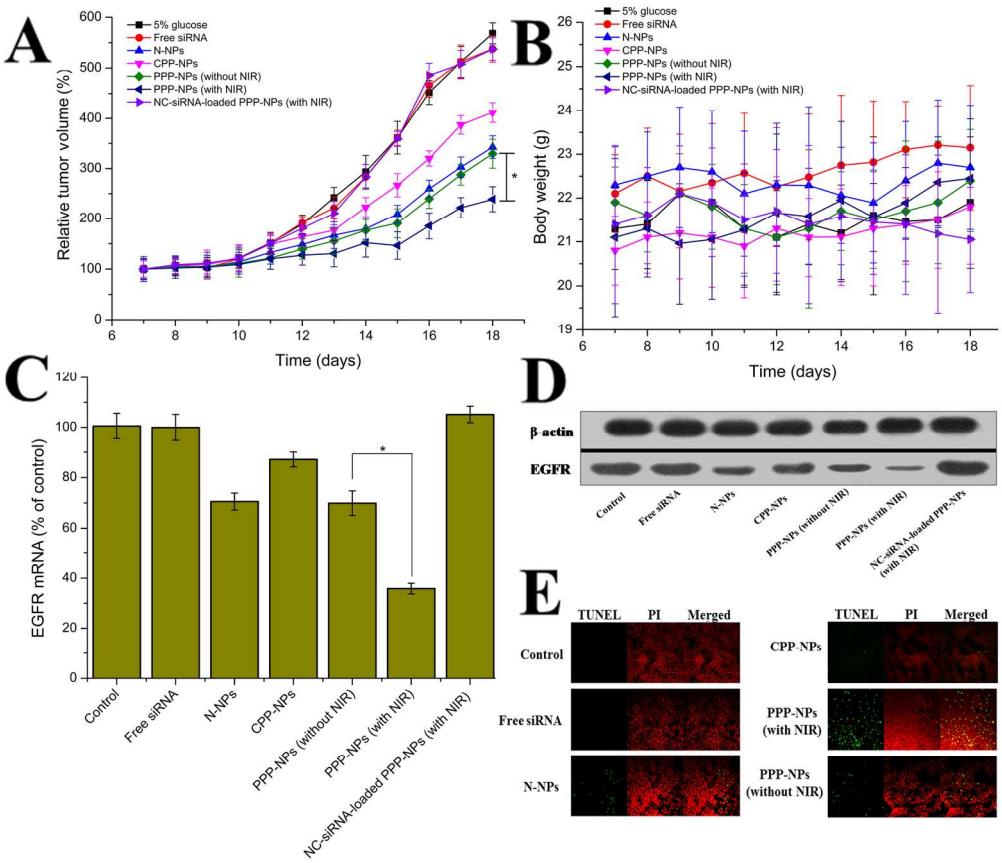

Figure 9. Antitumor activity (A) and body weight changes (B) in MCF-7 tumour-bearing mice after treatment with 5% glucose and various NPs carrying siRNA. The data are presented as the means ± SD (n = 6). The expression of EGFR mRNA (C), protein (D) and TUNEL detection of apoptotic cells (E) in tumours was detected 24 h after the last administration. The data are presented as the means ± SD (n = 3). * indicates P< 0.05.
85x73mm (600 x 600 DPI)